ISSN 1392-2114 ULTRAGARSAS (ULTRASOUND), Vol. 63, No.4, 2008.

Comparison of simulations of ultrasonic fields of rectangular transducer

M. Gresevičius, E. Jasiūnienė, L. Mažeika

Prof. K. Baršauskas Ultrasound Research Institute,
of Kaunas University of Technology, Lithuania

Abstract:
Objective of this study was to compare the simulated ultrasonic fields of rectangular transducer obtained by two different techniques. The fields of elementary rectangular transducers were obtained by means of two different impulse response methods (FMIR and LWIR). Ultrasonic fields in a transmission mode excited by a Gauss shaped signal of 10MHz and 5 MHz transducers with different dimensions (length 5 mm, width – 2 mm, 1 mm and 0.7 mm) were simulated. In order to classify methods performance duration of calculations were measured. The performed simulations show that in a near field zone the results obtained by both methods match very well, but with the distance from the transducer the normalized root mean squared deviation increases, but never exceeds 10%. Calculations performed by the FMIR method are about 2.5 times faster compared to the LWIR method. In the FMIR method dynamic sampling in the time domain is used, this enables to keep non-increasing uncertainty versus the distance from a transducer plane contrarily to the LWIR method the uncertainty of which increases with a distance.
Keywords: simulations, ultrasonic field, radial array.

Introduction

Calculations of the acoustic fields radiated by rectangular ultrasonic transducers have been a subject of numerous investigations [1-8], however main disadvantage of these methods is the fact that they are relatively slow, mainly due to the need of small sampling steps in space and time domains at high frequencies. The impulse response approach was used for calculation of acoustic fields of rectangular transducers also by several authors [3,4,8]. In these works two different impulse response methods were investigated. One of the methods was implemented using Lockwood and Willete [4] (LWIR) approach and the second one was fast modification of impulse response (FMIR) method described in [9].

The objective of the present paper is to compare two different impulse response methods and to estimate reliability of the results obtained by these methods.

The fast technique for calculation of ultrasonic field of rectangular transducer method approach

In many articles [1,8-10] it was shown that in the case of piston like vibration of the transducer surface the pulse response $h(t,x,y,z)$ at a given time and observation point is proportional to the angle of the arc created by circular equidistant lines intersecting with the transducers face (Fig. 1). Distribution of the acoustic pressure can be found from the expression

$$p(t,x,y,z)=\rho\frac{\partial h(t,x,y,z)}{\partial t}\otimes u(t), \qquad (1)$$

where ρ is the density of the medium, $u(t)$ is the waveform of the particle velocity of the transducer surface and the symbol $\otimes$ denotes convolution operation.

In order to calculate the impulse response $h(t,x,y,z)$ of the ultrasonic field generated by a transducer at some space point $P(x,y,z)$ it is necessary to find out the angles of the arc created by equidistance lines intersecting the with transducers surface at each time instance. In work [9] and many others it was demonstrated that for a circular transducer these angles can be found analytically. In the case of numerical solutions it can be done for any arbitrary shape of a planar transducer [8, 10], including the rectangular transducer.

The meaning of these equidistant lines for the case of the rectangular transducer is explained in Fig. 1. There can be an unlimited number of the equidistant lines corresponding to the time instances $t\in[t_1,t_2]$, $t_1=r_1/c$ corresponds to the arrival time of the waves generated by a closest elementary segment of the transducer surface and correspondingly $t_2=r_2/c$ to the farthest. The total number of these lines used in the calculation depends on the sampling interval in the time domain Δt.

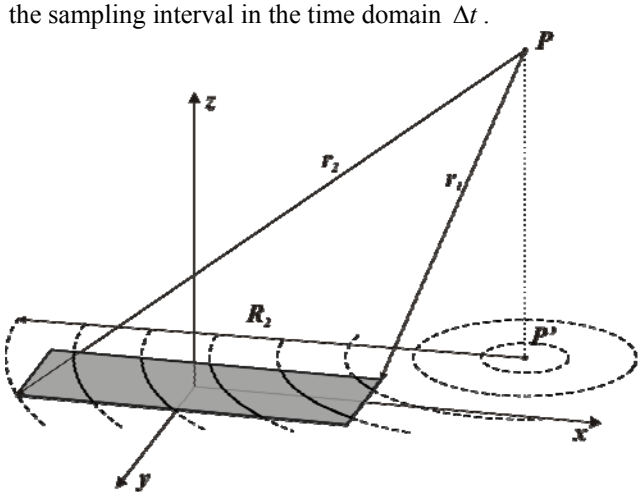

Fig. 1. **Explanation of the equidistant lines for the case of a rectangular transducer.**

It is easier to calculate the angle of the arc intersecting with the surface of the transducer in polar coordinates with the centre at the point *P* projection (Fig. 2).

Then the velocity potential can be expressed as

$$h(t,x,y,z)=\frac{c}{2\pi}\sum_{i=1}^{N(t)}\left[\Phi_2^{(i)}(t)-\Phi_1^{(i)}(t)\right], \qquad (2)$$

where $N(t)$ is the total number of arc segments for the observation point $P(x,y,z)$ intersecting with transducers boundaries for a given time instant, $\Phi_1^{(i)}(t)$ and $\Phi_2^{(i)}(t)$ is in and out angles for the equidistant line corresponding to the time instant t. It is necessary to state that the equidistant line for an arbitrary selected point can cross the contour of the transducer several times. In the case of the rectangular transducer the maximal possible number of cross-section points is 8. This procedure must be repeated for all time instant $t \in [t_1, t_2]$.

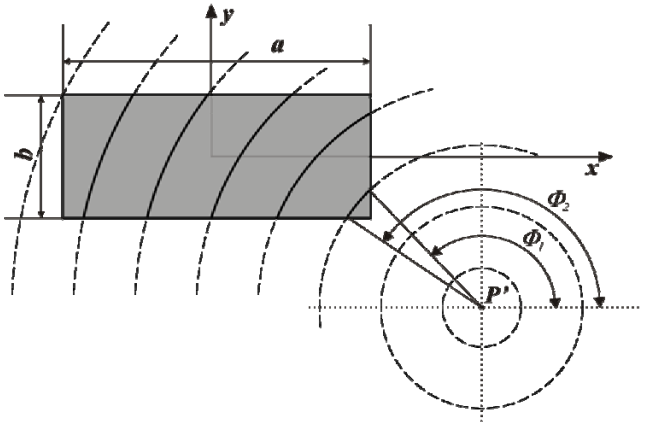

Fig. 2. **Explanation of in and out arc angles Φ_1 and Φ_2 used in calculation of velocity potential.**

However this rather simple approach possesses one very essential disadvantage. The relatively high frequencies (up to 10MHz) lead to a rather small sampling step in space and time domains and as a consequence to the huge number of points at which the calculation should be performed. So, calculation of the whole field requires a long time of processing. Additionally, the time instants t_1, t_2 of the arrival wave from the closest and the farthest points of the transducer surface become closer to each other for spatial points situated at bigger distances, that is the time interval $\Delta t_{12} = t_2 - t_1$ reduces with a distance. In order keep the same accuracy in the pulse response calculation, the sampling step in the time domain should be smaller for points situated at bigger distances from transducers. In conventional pulse response techniques the constant sampling step in the time domain is used. This leads to the over-sampling at close distances and as a consequence to the long calculation time or loss of the accuracy at far distances.

So, in order to reduce the computation time and to increase the model accuracy it was proposed to use the sampling step in the time domain dependant on a distance as it was described in [1] paper.

Lockwood and Willete impulse response approach

According to the method purposed by Lockwood and Willete [4] in a rectangular transducer case, the impulse response for any field point (x, y, z) can be found. First of all for any spatial point (x, y, z) its projection $O' = (x, y, 0)$ on the plane of the rectangular transducer is found (Fig. 3). The rectangular transducer is subdivided into four rectangles, each with the corner at O′. The field of the rectangular transducer is obtained by combining the field of the four rectangles. If O′ is outside the rectangular transducer, the rectangle is enlarged to include it and the added rectangles are subtracted.

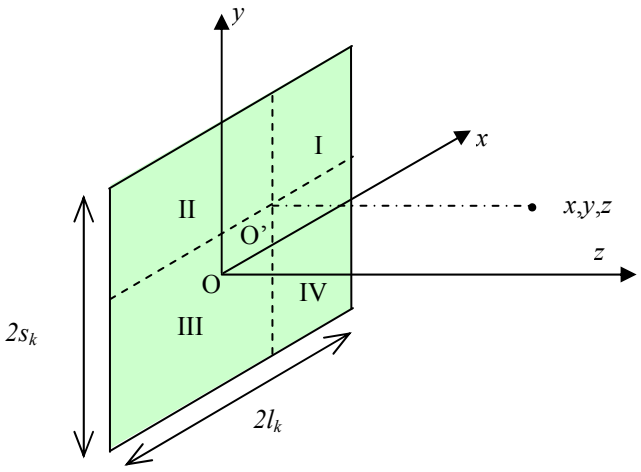

Fig. 3. **Subdivision of the rectangular transducer into four rectangles.**

The spatial impulse response is expressed as:

$$h(x,y,z,t) = -\frac{c}{2\pi}\sum_{k=1}^{4} \pm \left\{ \frac{\pi}{2}\left[H(t-t_{1k}) - H(t-t_{4k})\right] - \right.$$
$$- \arccos\left\{ \frac{S_k}{\sqrt{c^2(t-t_{2k})^2 - z^2}} \right\} \times \left[H(t-t_{2k}) - H(t-t_{4k})\right] -$$
$$\left. - \arccos\left\{ \frac{l_k}{\sqrt{c^2(t-t_{3k})^2 - z^2}} \right\} \times \left[H(t-t_{3k}) - H(t-t_{4k})\right] \right., \quad (3)$$

where s_k is the length of the short side of the rectangle, l_k is the length of the long side of the rectangle, $H(t)$ is the Heaviside function, $t_{1k} = z/c$ is the time of flight of the plane wave from the transducer to the observation point; $t_{2k} = \frac{\sqrt{z^2 + s_k^2}}{c}$ is the time of flight of the signal from the nearest edge of the transducer to the observation point; $t_{3k} = \frac{\sqrt{z^2 + l_k^2}}{c}$ is the time of flight of the signal from the farthest edge of the transducer to the observation point; $t_{4k} = \frac{\sqrt{z^2 + s_k^2 + l_k^2}}{c}$.

The acoustic field can be expressed as:

$$p_i(x,y,z,t) = \rho \frac{\partial}{\partial t}\left[v(x,y,z,t) * h(x,y,z,t)\right]. \quad (4)$$

where ρ is the density of the medium, v_i is the particle velocity, $*$ denotes convolution.

The complete field of the transducer is expressed as the sum of the fields of the rectangles:

$$p(x,y,z,t) = \sum_{i=1}^{N} p_i(x,y,z,t). \quad (5)$$

Comparison results

Practical implementations of both methods have been made in MatLAB application. This eliminates differences that may occur due to different application media.

The ultrasonic fields of a rectangular transducer were calculated in two perpendicular planes *x*0*z* and *y*0*z* (Fig.5–10). The calculations were carried out using the parameters given in Table 1. The waveform of the 10 MHz excitation signal is shown in Fig. 4.

Table 1. **Parameters used in simulations**

Parameter	Value
The dimension of the transducer in *y* direction, mm	5
The dimension of the transducer in *x* direction, mm	2; 1; 0.7
The ranges of field calculation in *y* and *x* directions, mm	-5÷5
The range of field calculation in *z* direction, mm	0÷35
The step in *y* and *x* directions, mm	0.1
The step in *z* direction, mm	0.1
The velocity of ultrasound in medium, m/s	1500
The frequencies, MHz	5; 10
The sampling in the time domain, ns	1; 2

Both models gave results that look very similar, only in the field obtained by the LWIR method the pattern of numerical noise can be observed (Fig. 5b, Fig. 6b and Fig. 7b). Also the length of the near field zone is slightly shorter compared to the FMIR method. In order to observe difference of the results the cross-sections of the fields in different planes are presented in Fig. 11 - Fig. 13. The near field zones related to the transducer width and length can be identified clearly by the amplitude maximums (Fig.8, Fig.10). Some "anomaly" in the direct beam field obtained by the LWIR technique can by observed in Fig.9 and Fig.10.

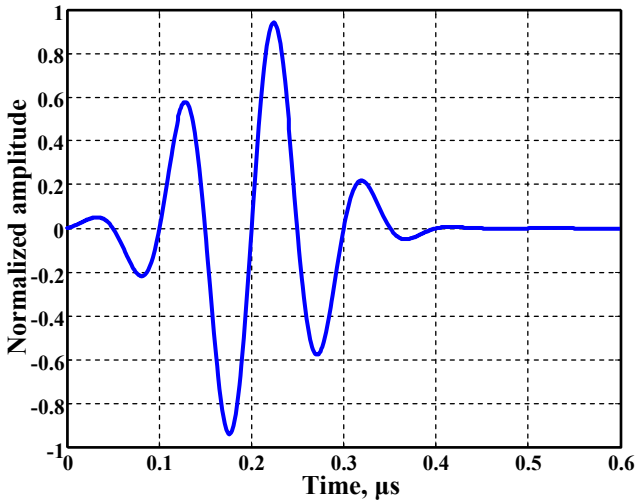

Fig. 4. **Normalized 10 MHz signal used for excitation of ultrasound transducer in calculations**.

This "anomaly" probably is caused by the insufficient sampling interval in the time domain and becomes more visible when the transducer *x* dimension gets smaller.

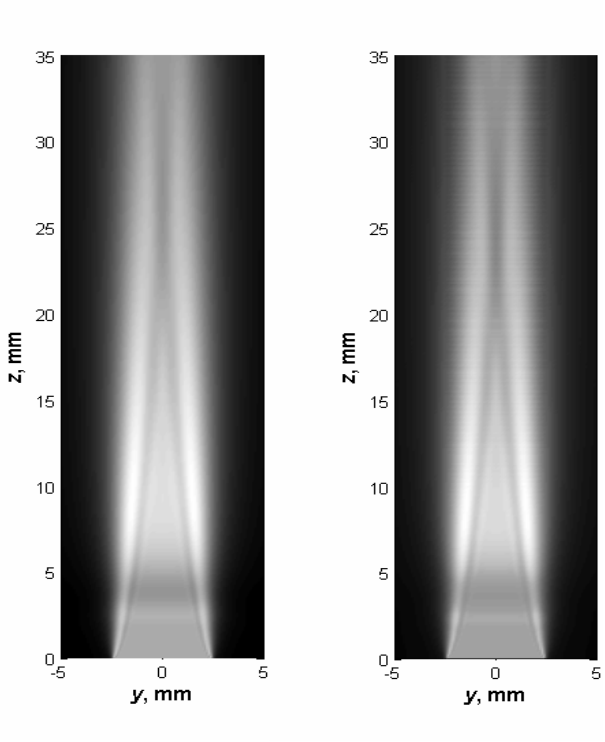

a b

Fig. 5. **Calculated ultrasound field of the rectangular transducer 5x2 mm in a transmission mode: a - using FMIR method; b - LWIR method in *y*0*z* plane. The excitation signal frequency 10 MHz.**

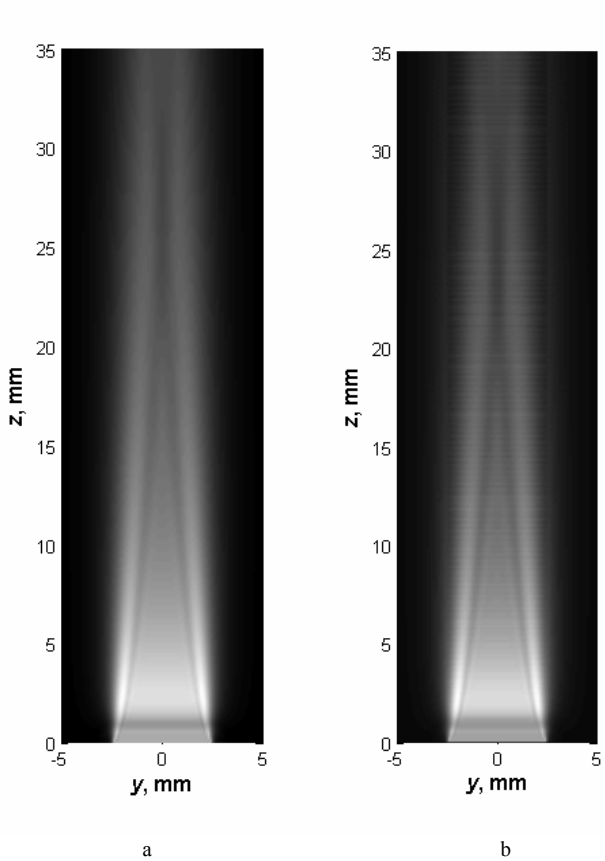

a b

Fig. 6. **Calculated ultrasound field of the rectangular transducer 5x1 mm in a transmission mode: a - using FMIR method; b - LWIR method in *y*0*z* plane. The excitation signal frequency 10 MHz.**

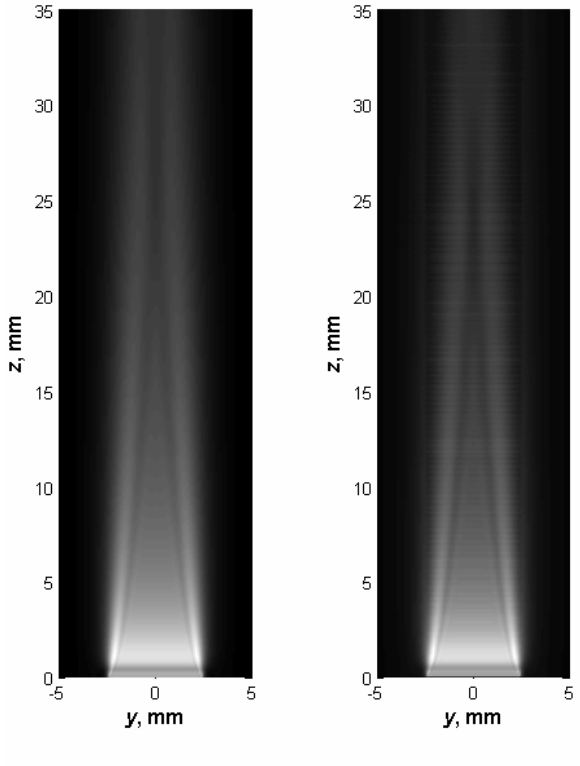

a b

Fig. 7. **Calculated ultrasound field of the rectangular transducer 5x0.7 mm in a transmission mode: a – using the FMIR method; b – the LWIR method in *y*0*z* plane. The excitation signal frequency 10 MHz.**

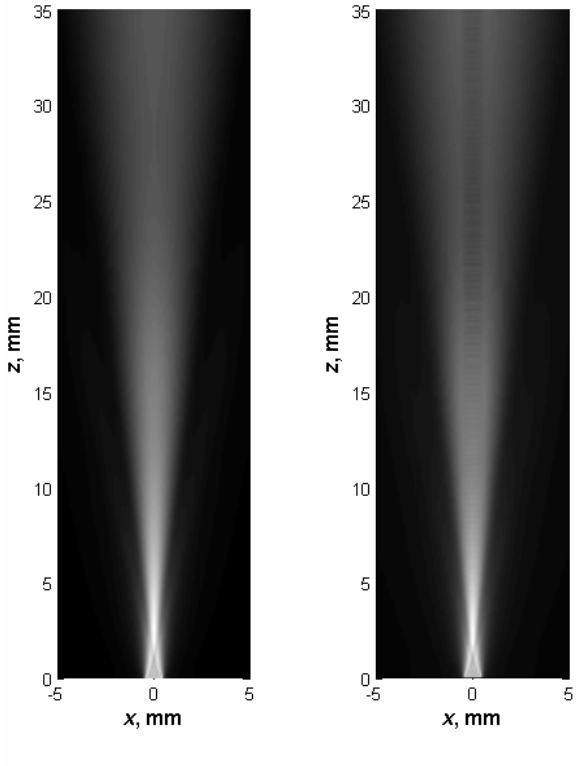

a b

Fig. 9. **Calculated ultrasound field of the rectangular transducer 5x1 mm in a transmission mode: a - using the FMIR method; b – the LWIR method in *x*0*z* plane. The excitation signal frequency 10 MHz.**

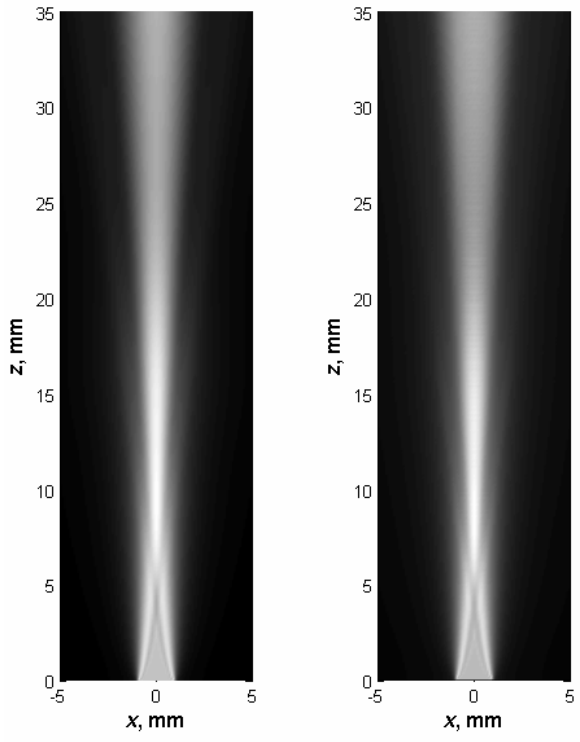

a b

Fig. 8. **Calculated ultrasound field of the rectangular transducer 5x2 mm in a transmission mode: a - using the FMIR method; b – the LWIR method in *x*0*z* plane. The excitation signal frequency 10 MHz.**

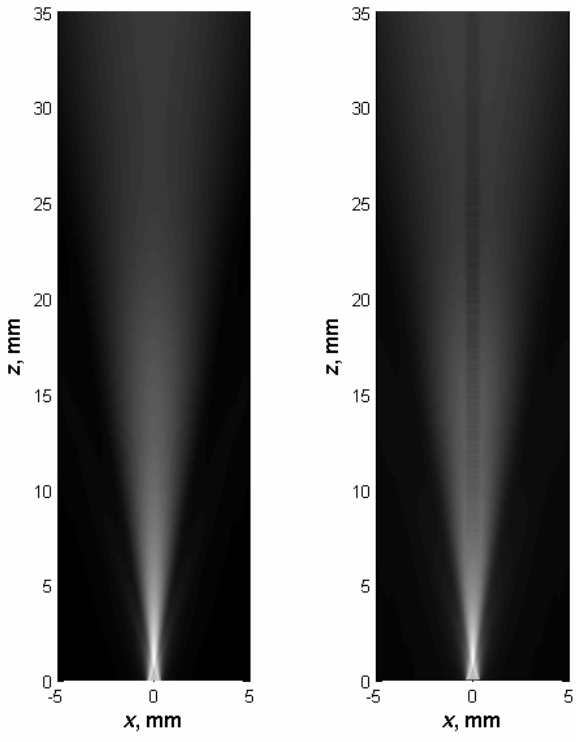

a b

Fig. 10. **Calculated ultrasound field of the rectangular transducer 5x0.7 mm in a transmission mode: a - using FMIR method; b – the LWIR method in *x*0*z* plane. The excitation signal frequency 10 MHz.**

It may be noted that in the near-field zone (Fig. 11) located close to the transducer surface, the results obtained by both methods overlap very well, however the difference increases for bigger distances (Fig. 12 Fig. 14).

The comparison shows that the LWIR method, demonstrates similar problems as the basic FMIR method without optimization, e.g. some systematic error in the area of transducer projection ("inside" the direct beam) which can be observed in the cross-section perpendicular to the transducer axis (Fig.12) and in cross-sections along the transducer axis (Fig. 13). The proposed dynamic sampling frequency used in the FMIR technique enables to avoid these errors as it is demonstrated by a smooth increase of the field in the boundary region between "inside" and "outside" of the direct beam.

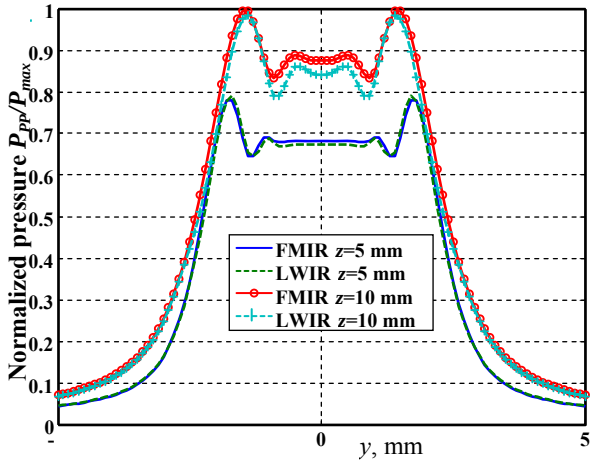

Fig. 11. **Normalized acoustic pressure distribution of the 5x2 mm transducer obtained by FMIR and LWIR methods at z= 5 mm; 10 mm when x= 0 and y= -5÷5 mm, the frequency 10 MHz.**

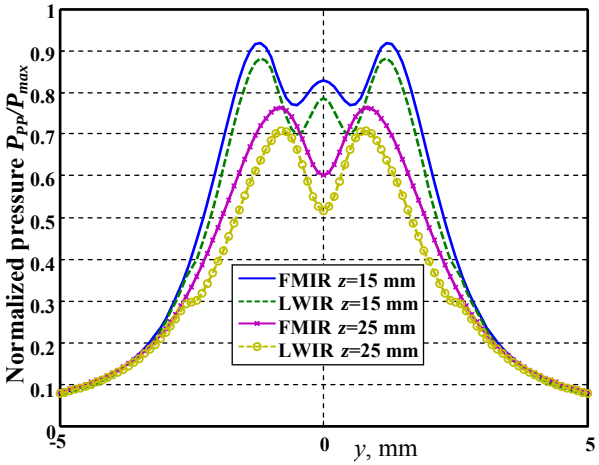

Fig. 12. **Normalized acoustic pressure distribution of the 5x2 mm transducer obtained by FMIR and LWIR methods at z= 15 mm; 25 mm when x= 0 and y= -5÷5 mm, the frequency 10 MHz.**

For estimation of differences between the results obtained by FMIR and LWIR methods, the global normalized root mean squared deviation was calculated for calculated field in different cross-sections according to,

$$s_g = \sqrt{\frac{\sum_{i=1}^{n}\left(p_{FMIR_i} - p_{LWIR_i}\right)^2}{n}} \Big/ P_{g\max} \times 100\%, \quad (6)$$

where p_{FMIRi} is the maximum peak to peak pressure value at i-th spatial point calculated by the FMIR method, p_{LWIRi} is the maximum peak to peak pressure value at i-th spatial point calculated by the LWIR method, n is the number of elements used for calculation of deviation, $P_{g\ \max}$ is the global maximum of peak to peak value of the acoustic pressure.

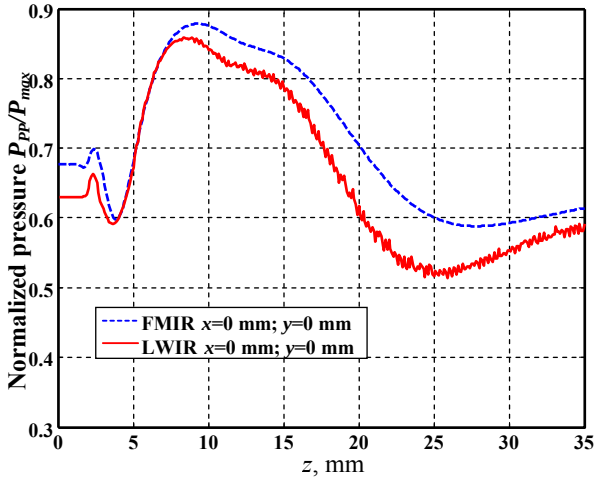

Fig. 13. **Normalized acoustic pressure distribution of the 5x2 mm transducer obtained by FMIR and LWIR methods at z= 0÷35 mm when x= 0; y= 0 mm; the frequency 10 MHz.**

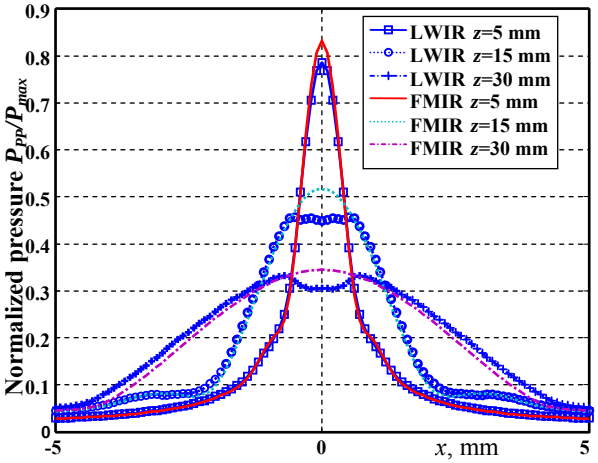

Fig. 14. **Normalized acoustic pressure distribution of the 5x1 mm transducer by FMIR and LWIR methods at z= 5 mm; 15 mm; 30 mm when x= -5÷5 mm; y= 0 mm; the frequency is 10 MHz.**

However, in cross-sections that are at further distances from the field maximum position and the relative pressure level is low, Eq. 6 does not present clearly difference between two methods, therefore, the local normalized root mean squared deviation is calculated:

$$s_l = \sqrt{\frac{\sum_{i=1}^{n}\left(p_{FMIR_i} - p_{LWIR_i}\right)^2}{n}} \Big/ P_{l\max} \times 100\%, \quad (7)$$

where $P_{l\ \max}$ is the maximum peak to peak value of the acoustic pressure in the field cross-section under analysis. The obtained deviation values are presented in Table 2 and demonstrate similar regularities, that is, the difference between two techniques is more strongly expressed at bigger distances.

The deviations were calculated separately in different transducer beam areas "inside" and "outside" direct beam

also (Table 3). The "outside" direct beam deviations are less than 1.5%, but "inside" deviations can be up to one order bigger. This demonstrates that there are some systematic errors in the LWIR technique inside the direct beam area.

In order to evaluate the calculation speed, the modelling time was measured in each case (Table 4). The version of the FMIR method which exploiting dynamic sampling was used. The modelling using LWIR method was performed using two different sampling intervals in the time domain. The duration of the first one was optima for the FMIR method at close distances, the second one optimal at the furthest spatial points from the transducer plane.

Table 2. **Local and global normalized root mean squared deviations in different cross-sections of calculated acoustic field planes, the frequency 10 MHz.**

Coordinate z, mm		s_g (global), %	s_l (local), %
$y0z$ plane transducer 5x2 mm	5	0.89	1.13
	10	2.51	2.52
	15	3.92	4.27
	25	5.24	6.87
$x0z$ plane. transducer 5x1 mm	5	0.51	0.69
	15	0.96	3.16
	30	0.97	3.45

Table 3. **Normalized root mean squared deviations in different spatial sections according to transducer boundary projections, the frequency 10 MHz**

Coordinate z, mm		s_g outside transducer projection, %	s_g inside transducer projection, %
$y0z$ plane transducer 5x2 mm	5	0.25	1.24
	10	0.51	3.54
	15	0.72	5.53
	25	0.89	7.39
$x0z$ plane. transducer 5x1 mm	5	0.21	2.36
	15	0.53	5.25
	30	1.33	3.56

Table 4. S**imulation times of acoustic fields FMIR and LWIR methods x= -5÷5 mm; y= 0 mm; z= 0÷35 mm generated by the rectangular 5x2mm transducer, the frequency 10 MHz, the number of spatial points 17.9 k.**

Method	Sampling interval Δt, ns	Simulation time, s
FMIR	Dynamic: 1 ns, at z= 0 mm; 0.086 ns, at z= 35 mm	182
LWIR	1 ns	471
	0.086 ns	6919

Conclusions

The obtained results of the normalized root mean squared deviations show that they are up to ten times higher in the transducer direct beam zone, compared to the area "outside" the direct beam. This noticeable difference occurs due to insufficient sampling in the time domain. The FMIR method employs dynamic sampling in the time domain that is more accurate comparing to the LWIR method.

It was demonstrated that in average the FMIR method is at least 2.5 times faster compared to the LWIR method. However, in the case of bigger distances the FMIR method is more than 30 times faster if the same accuracy is required.

Acknowledgements

The part of this work was sponsored by the European Union under the Framework-6 TROY ("Endoscope Capsule using Ultrasound Technology") project. TROY is collaboration between the following organizations: IAITI (Portugal), SC IPA SA (Romania), Dunvegan (UK), AGT (Italy), Ardoran (Estonia), Artica (Spain), Labor (Italy), UI of KTU (Lithuania), UMF Cluj – Napoca (Romania).

The Project is coordinated and managed by IAITI (Portugal) and is partly funded by the EC under the programme ref.:FP6-2004-SME-COOP-33110-TROY.

References

1. **Mažeika L., Gresevičius M.** The fast technique for calculation of ultrasonic field of rectangular transducer. ISSN 1392-2114 Ultragarsas (Ultrasound), 2008. Vol. 63. No. 4.
2. **Jasiūnienė E., Kažys R., Mažeika L.** Simulations of ultrasonic fields of radial ultrasonic array. ISSN 1392-2114 Ultragarsas (Ultrasound). 2007. Vol. 62. No. 2.
3. **Piwakowski B. and Sbai K.** A new approach to calculate the field radiated from arbitrarily structured transducer arrays. IEEE Transactions on Ultrasonics, Ferroelectrics, and Frequency Control. March 1999. Vol. 46. No. 2. P. 422-440.
4. **Lockwood J.C. and Wilette J.G.** High-speed method for computing the exact solution for the pressure variations in the near field of a baffled piston. JASA. 1973. Vol. 53. No.3. P. 735-741.
5. **Cahill M. D. and Baker A. C.** Numerical simulation of the acoustic field of a phased-array medical ultrasound scanner. JASA. 1998. Vol. 104. No 3. P. 1274-1283.
6. **Jensen. J. A.** A new approach to calculating spatial impulse responses. Ultrasonics Symposium. Vol. 2. 1997. P. 1755-1759.
7. **Robinson D. E., Lees S., Bess L.** Near field transient radiation patterns for circular pistons. IEEE Transactions on Acoustics, Speech, and Signal Processing. December 1974. Vol. ASSP-22. No.6. P. 395-403.
8. **Mažeika L., Cicėnas V.** The method for the calculation of ultrasonic fields of planar free form transducers. Ultragarsas. 2001. Vol. 41. No.4. P. 12-17.

M. Gresevičius, E. Jasiūnienė, L. Mažeika

Ultragarsinių stačiakampių keitiklių sukuriamų laukų skaičiavimo metodų palyginimas

Reziumė

Ultragarsinių stačiakampių keitiklių laukams modeliuoti naudojami metodai turi ir pranašumų, ir trūkumų. Šio darbo tikslas – palyginti modeliavimo rezultatus, gautus dviem skirtingais metodais, ir įvertinti šių metodų rezultatų patikimumą. Vienas iš metodų yra impulsinės reakcijos metodas, kitas - žinomo difrakcinio metodo versija, skirta stačiakampio keitiklio laukui greitai apskaičiuoti. Metodams nuodugniai palyginti buvo sumodeliuoti skirtingų dažnių ir matmenų keitiklių sukuriami ultragarsiniai laukai. Buvo tiriami mažų matmenų stačiakampio ultragarsinio keitiklio (ilgis – 5 mm, plotis – 2 mm, 1 mm) sukuriami laukai. Keitiklis buvo žadinamas 10 MHz ir 5 MHz dažnio Gauso formos signalu, buvo parinkti vienodi laiko ir erdvės diskretizavimo žingsniai. Metodų efektyvumui nustatyti buvo matuojami modeliavimo laikai. Tyrimo rezultatai parodė, kad metodų skirtumai reiškiasi tolimajame lauke, tačiau standartiniai kvadratiniai nuokrypiai neviršija 10 %. Naudojant sparčiąją difrakcinio metodo versiją, skaičiavimai atliekami apie du kartus sparčiau nei impulsinės reakcijos metodu. Pritaikius šiai versijai dinaminį diskretizavimo laike žingsnį, neapibrėžtis tolstant nuo keitiklio plokštumos nekinta, priešingai nei impulsinės reakcijos metodo, kur neapibrėžtis didėja tolstant nuo keitiklio plokštumos.

Pateikta spaudai 2009 12 15